JOURNAL OF SPACECRAFT AND ROCKETS
Vol. 58, No. 5, September–October 2021

Impact of Electrostatic Perturbations on Proximity Operations in High Earth Orbits

Kieran Wilson* and Hanspeter Schaub†
University of Colorado Boulder, Boulder, Colorado 80301

https://doi.org/10.2514/1.A35039

A range of upcoming missions propose to rendezvous in high Earth orbits, including the geostationary orbit region. This region is known to periodically experience high levels of electrostatic charging, which can result in perturbing intercraft forces and torques during close-proximity operations on the order of tens of meters. A range of proximity operations with a nonoperational target are modeled to evaluate the impact of electrostatic force and torque perturbations as a result of spacecraft charging. Perturbing electrostatic torques are evaluated using the multisphere method and result in the target body rotating, requiring the servicer to maintain its relative position by translation. Electrostatic perturbations are found to be significant, with potentials on the order of 1000 V resulting in larger perturbing torques than solar radiation pressure for this model. Electrostatic perturbations exist even in cases where both spacecraft are at the same potential. Record charging conditions lead to target rotational rates over 0.1 deg/s during a nominal rendezvous. Target rotations require increases in fuel consumption for rendezvous and proximity operations, over 10 times more than a solar radiation pressure-induced torque, and present additional challenges associated with maneuvering in proximity to a tumbling target in a highly coupled and nonlinear dynamic environment.

Nomenclature

C	=	capacitance, F
F	=	force vector
F_c	=	Coulomb force
I	=	inertia matrix
K_c	=	Coulomb's constant,
L	=	torque vector, external torque vector
n	=	orbital mean motion
q_i	=	charge on body i, C
u	=	control effort, m/s^2
V	=	electrostatic potential, V
ϵ_0	=	vacuum permittivity, $\approx 8.854 \times 10^{-12}$, F/m
ω	=	angular velocity vector

I. Introduction

AFTER decades of research, robotic orbital servicing is finally moving from a promising, albeit futuristic, concept to reality. The Mission Extension Vehicle (MEV-1) from the SpaceLogistics subsidiary of Northrop Grumman was launched as the first commercial satellite servicing mission in 2019. It successfully rendezvoused with Intelsat 901 in the geostationary orbit (GEO) graveyard, physically latching onto Intelsat 901 and assuming station keeping and attitude control responsibilities for the fuel-depleted communications satellite. This effectively adds years of useful life to the otherwise functional communications satellite, and introduces the era of commercial orbital servicing [1]. Similarly, NASA is planning a robotic refueling demonstration of the Landsat 7 spacecraft, a vehicle that was never designed for servicing, within 3 years [2]. These missions, as well as a range of related concepts from servicers to space tugs, illustrate a rapid maturation of robotic servicing technologies dependent on automated rendezvous operations.

In a related field, the need for active debris removal in all orbital regimes is becoming more pressing with every collision and near miss. The addition of tens of thousands of spacecraft in mega-constellations will only further heighten the need to remove potentially hazardous debris objects [3]. Such operations, whether for servicing or debris mitigation, will inevitably require automated rendezvous. However, few servicing operations have ever been conducted in orbit, with notable exceptions for space stations and the Hubble Space Telescope. The majority of these servicing missions were conducted by humans, and none other than MEV-1 has occurred in GEO. Additionally, all of these rendezvous maneuvers occurred with well-characterized, cooperative targets, which cannot be assumed for a debris remediation or repair mission.

Spacecraft develop electrostatic charges through interactions with the space environment, where currents arise primarily through solar-induced photoelectric electron emission, bombardment by ions and electrons in the ambient plasma, and the backscattered and secondary electron emissions that result from those impacts [4]. Although spacecraft charging can occur in low Earth orbit (LEO), particularly in orbits that cross the auroral regions, these events are typically limited to kilovolt levels and are relatively fleeting [5]. However, beyond LEO, environmental plasma parameters become more conducive to heightened and sustained spacecraft charging. The Applications Technology Satellite 6 mission, for instance, recorded potentials as high as −19 kV in GEO [6]. Additionally, the increasing debye length that comes with sparser, more energetic plasmas at higher altitudes results in less shielding of electrostatic charges, and therefore greater electrostatic interactions between spacecraft operating in close proximity. In GEO regions, for instance, Debye lengths are typically on the order of 100–1000 m, compared with centimeters at LEO [7].

A significant body of prior work focuses on the use of controlled spacecraft charging to achieve desired intercraft forces and torques. These concepts cover using electrostatic forces for propellant-less Coulomb formation flying [8,9] as well as related concepts, like the electrostatic tractor for active debris detumbling and reorbiting in GEO [10,11]. However, relatively little work focuses on the impacts of natural charging on spacecraft relative motion, although King et al. [8] found that significant torques are generated by intercraft electrostatic forces as a result of natural charging in a formation flying context. With increasing interest in rendezvous in high-altitude orbits prone to charging—particularly from GEO to cislunar space—it will become necessary to assess the impact of charging on relative motion dynamics to ensure mission success during proximity operations and rendezvous.

Received 9 December 2020; accepted for publication 12 February 2021; published online 27 May 2021.

*Graduate Research Assistant, Ann and H.J. Smead Aerospace Engineering Sciences Department. Member AIAA.

†Glenn L. Murphy Endowed Chair, Ann and H.J. Smead Aerospace Engineering Sciences Department. Fellow AIAA.

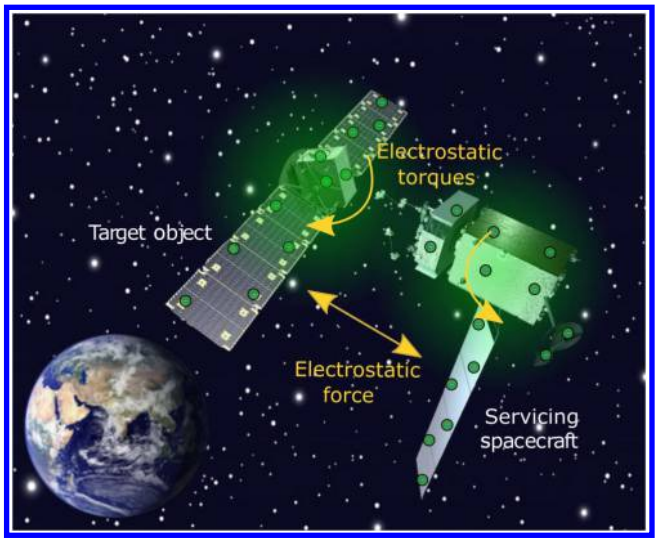

Fig. 1 Concept figure of a high Earth orbit servicing mission perturbed by electrostatic forces and torques.

This work analyses the impact of charged spacecraft on the dynamics of close proximity operations between an active spacecraft and an inert or disabled target object flying tens of meters apart, as seen in Fig. 1. This paper is organized as follows: first, the general frequency of spacecraft charging in high Earth orbits is discussed for context. Next, a method to rapidly evaluate electrostatic forces and torques is discussed, followed by the application of that technique in developing a six-degree-of-freedom two-craft simulation of a controlled servicer and two types of inert target vehicle. Results from simulations with different spacecraft geometries for both rendezvous trajectories and relative station keeping are discussed, and the results compared to perturbations resulting from solar radiation pressure (SRP). Finally, a rendezvous scenario is used as an alternative demonstration of electrostatic charging impacts on relative motion.

II. Frequency of Charging

Spacecraft charging in the GEO region is known to occur more frequently during enhanced electron fluxes associated with geomagnetic storm time conditions [12]. The global K_p index is a widely used measure of geomagnetic disturbance, evaluated every 3 h on a 0–9 scale, with higher values indicating a more disturbed magnetic field. Data for the K_p index every 3 h for the last four solar cycles, spanning October 1964 to December 2019, were obtained from Ref. [13].

For the majority of measurements over the last four solar cycles, the K_p index was at a value of 2 or lower, as seen in Fig. 2, indicating relatively quiet geomagnetic conditions. However, 36% of measurements recorded $K_p = 3$ or higher, indicating a somewhat disturbed geomagnetic environment, with approximately 6% of measurements exceeding $K_p = 4$, indicating a storm condition. These events are concentrated around periods of solar maximum, and a 30 day sliding window applied to the data reveals some 30 day periods with over 15% of measurements at $K_p > 4$. Charging events can still occur during periods of quiet ($K_p < 3$), but tend to be less likely, less intense, and less prolonged [12].

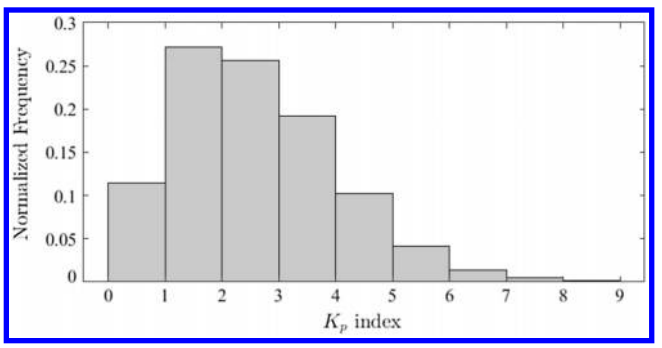

Fig. 2 Distribution of K_p index values over the last four solar cycles (October 1964 to December 2019).

Ozkul et al. [12] found that times of elevated K_p are associated with a 30% chance of experiencing charging events, compared with low single-digit probabilities during low K_p periods. Ultimately, this suggests that, although severe electrostatic charging that could result in significant perturbations during proximity operations is rare, periods with frequent charging events can occur, warranting further consideration of the impacts of electrostatic charging on proximity operations.

Furthermore, it is important to note that these potentials refer to surface charging, and although guidelines for spacecraft design recommend that all components be grounded to the frame, this may not always apply. Some spacecraft may have been launched without such continuity, whereas others may have had components degrade in the space environment to no longer be conducting. Olsen et al. [14] found that periods of low charging (< -20 V frame potentials) could have ungrounded components, such as pieces of Kapton, which experience kilovolt-level potentials. Therefore, it may be possible for some spacecraft components to charge to significant levels even when the spacecraft frame potential is negligible. However, for this work, continuously conducting spacecraft are assumed, and so all surfaces hold an equal potential. This is a suitable assumption for high Earth orbit or geosynchronous spacecraft, as their construction guidelines require a continuously conducting outer surface to avoid differential charging among components [15,16].

III. Problem Formulation

A. Spacecraft Models

The prototypical scenario considered in this paper involves a servicer with two solar arrays (loosely based on the Northrop Grumman MEV-1 GEO servicing vehicle, and referred to as the "two-panel model") rendezvousing with an uncooperative target. One of the next-generation Geostationary Operational Environmental Satellite (GOES) spacecraft (the GOES-R) of the National Oceanic and Atmospheric Administration (NOAA) is chosen as an example target; these craft are crucial for weather forecasting in space and on Earth, and cost over $2.5 billion each [17]. They also operate on traditional chemical propellants, and so it is reasonable that NOAA may want to service or refuel them in the future to extend their service lives. Significant public data are available for this spacecraft, allowing a better estimation of inertia and mass properties than can be achieved for most commercial spacecraft. The two-panel model is considered as an alternative spacecraft with symmetry about the docking axis. These spacecraft shapes are chosen because they contain representative geometries that might be encountered on orbit, and they provide both a symmetric and asymmetric configuration. The latter argument about symmetry is important because the center of charge (COC) and center of mass can be very different in a nonsymmetric configuration.

Publicly available photographs and published dimensions of each craft are used to construct method of moments (MOM) models [18], with an example GOES-R spacecraft model shown in Fig. 3 [17]. However, inertia properties are rarely published, and knowledge of the center of mass and the inertia matrix of the uncontrolled target is necessary to accurately model the impact of electrostatic forces and torques. Therefore, these properties are estimated using the following process.

A CAD model of the GOES-R spacecraft is developed using approximate vehicle and fuel tank dimensions from Ref. [17]. Published wet and dry masses are used to determine the mass of fuel onboard, which is then modeled as evenly distributed through each tank volume. The remaining dry mass is assumed to be evenly distributed through the spacecraft, excluding the tanks. This model is then used to calculate inertia properties and center of mass location. Although approximate, these numbers reflect a reasonable starting point for this analysis, where the goal is not to determine how a specific object will respond to electrostatic forces and torques, but instead to evaluate the general impact of these perturbations. For this

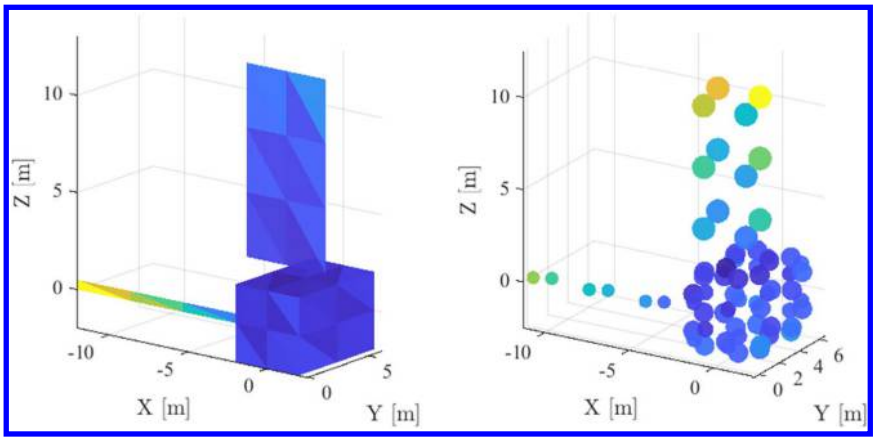

Fig. 3 GOES-R spacecraft approximated as an 80-element MOM finite element model (left) and an 80-sphere MSM model (right); spheres are colored according to surface charge density.

end-of-life servicing mission, the fuel tanks are assumed to be depleted.

B. Dynamics

The perturbations of interest occur over small separation distances on the order of tens of meters. Thus, the final stage of a rendezvous and docking process is considered, where the servicer slowly approaches a target vehicle and has brief target-relative hold periods to evaluate mission parameters before docking. Additionally, these effects are predominant in regions of high spacecraft charging, such as GEO. The combination of very close formation flight (tens of meters), large orbital radii with small eccentricities (a over 42,000 km; $e = 0.0001$), and relatively short time periods makes the dynamics well suited to linearization, and so Hill–Clohessy–Wiltshire (HCW) equations of relative motion are used [19]. The components a_x, a_y, a_z represent the Hill-frame components of acceleration contributed by perturbing forces, whether electrostatic or control thrust; n is the orbital mean motion:

$$\begin{aligned}\ddot{x} &= 3n^2x + 2n\dot{y} + a_x\\ \ddot{y} &= -2n\dot{x} + a_y\\ \ddot{z} &= -n^2z + a_z\end{aligned} \tag{1}$$

Two spacecraft are established as deputies relative to a virtual Keplerian chief orbiting in a GEO graveyard. The deputies exert mutual forces and torques due to electrostatic interactions such that they exhibit perturbed motion relative to the Keplerian chief frame $\mathcal{H}$. The first deputy, which represents the uncontrolled target for rendezvous, is initially located at the origin of the HCW frame, whereas the second spacecraft (the controlled servicer) is set at an initial position determined by the scenario under consideration.

Translational dynamics constitute only one part of the problem, however. The two spacecraft exert mutual torques on each other, which will perturb their attitudes. This has a strong impact on the servicer motion, as it must approach in a prescribed manner relative to the target object body frame. Thus, if the object is tumbling, the servicer needs to match this motion to maintain a body-fixed approach. The external torque vector L acting on each craft is related to the angular rotational vector ω of each body by

$$[I]\dot{\omega} = -\tilde{\omega}[I]\omega + L \tag{2}$$

where the tilde represents the skew-symmetric matrix operator equivalent to a vector cross product, and $[I]$ represents the inertia tensor [19]. Quaternions are used to represent attitudes, and the attitude of the servicer is prescribed to match the attitude of the target at each time step to simulate active relative attitude control of the servicer relative to the target object. At each time step, the translational states and rates are integrated using the CW equations, whereas Euler's equation of rotational motion is used to integrate rotational rates, and the quaternion differential equation of motion is used to integrate attitude states.

There are four relevant reference frames for this scenario: $\mathcal{N}$, an Earth-centered inertial frame; $\mathcal{H}$, an unperturbed co-orbiting origin point for the Hill frame; $\mathcal{T}$, a body-fixed frame on the target spacecraft; and $\mathcal{S}$, a body-fixed frame at the docking point on the servicer. The servicer attitude reference frame $\mathcal{T}$ is fixed to the docking point on the target, as would be expected for a servicing scenario. As the target spacecraft rotates due to perturbing torques, the reference location is also rotated in the HCW frame.

C. Multisphere Method for Electrostatic Force and Torque Evaluation

The electrostatic force for the simplest case between two point charges is provided by Coulomb's law, where forces are proportional to the product of the charge magnitudes (q_1 and q_2), and inversely proportional to the square of the distance between the charges (r) as

$$F_c = k_c \frac{q_1 q_2}{r^2} \tag{3}$$

where k_C is Coulomb's constant, defined as $k_c = 1/4\pi\epsilon_0 8.99 \times 10^9\ (\mathrm{N}\cdot\mathrm{m}^2)/\mathrm{C}^2$

The charge q of a physical object is related to the capacitance C by the voltage V:

$$q = VC \tag{4}$$

Therefore, if the voltage of an object is known, then the capacitance can be used to determine charge, which can then be used to determine the force acting between two bodies. However, objects in close proximity will exhibit mutual capacitance effects, which must be accounted for to accurately determine the total charge on each object. For the simplest 3-D case with two spheres in a pure vacuum, the potentials (V_1 and V_2) are used to determine the total charge on each sphere using the relation [20]:

$$\begin{bmatrix} q_1 \\ q_2 \end{bmatrix} = \underbrace{\frac{d}{k_c(d^2 - R_1R_2)}\begin{bmatrix} dR_1 & -R_1R_2 \\ -R_1R_2 & dR_2 \end{bmatrix}}_{C_V}\begin{bmatrix} V_1 \\ V_2 \end{bmatrix} \tag{5}$$

where d is the distance between each sphere center, and R_1, R_2 are the sphere radii.

If the capacitance of a spacecraft is known, then it can be approximated as a sphere with a radius that results in an equivalent capacitance. The self-capacitance of a sphere is given by the analytical expression:

$$C_{\text{sphere}} = 4\pi\epsilon_0 R \tag{6}$$

However, two spheres only roughly approximate the electrostatic forces between two spacecraft and fail to capture any of the torques

associated with the bodies; these limitations can be overcome with the use of multiple spheres. The multisphere method (MSM) quickly and accurately approximates the distribution of electric charge on a body through the use of a series of spheres [21]. Given the potential on each sphere and its location relative to all other spheres, it is possible to analytically compute the charge on each sphere:

$$\begin{pmatrix} V_1 \\ V_2 \\ \vdots \\ V_n \end{pmatrix} = k_c \begin{bmatrix} 1/R_1 & 1/r_{1,2} & \cdots & 1/r_{1,n} \\ 1/r_{2,1} & 1/R_2 & & 1/r_{1,n} \\ \vdots & \vdots & \ddots & \vdots \\ 1/r_{n,1} & 1/r_{n,2} & & 1/R_n \end{bmatrix} \begin{pmatrix} Q_1 \\ Q_2 \\ \vdots \\ Q_n \end{pmatrix}, \quad \boldsymbol{V} = [S]\boldsymbol{Q} \tag{7}$$

Here, $[S]$ denotes the elastance matrix, which is also the inverse of the capacitance matrix [18].

The total force acting on body 1, composed of charges q_j, is computed by summing the forces of each sphere in body 2 (charges q_i) on each sphere in body 1:

$$\boldsymbol{F} = k_c \sum_{j=1}^{n_1} q_j \left(\sum_{i=1}^{n_2} \frac{q_i}{r_{i,k}^3} r_{i,j} \right) \tag{8}$$

With the force between each pair of charges known, this formulation is readily extended to find the torque acting on each body:

$$L_O = k_c \sum_{j=1}^{n_1} q_j \left(\sum_{i=1}^{n} \frac{q_i}{r_{i,j}^3} r_i \times r_{i,j} \right) \tag{9}$$

The MSM is predicated on the knowledge of some property of the target body, whether charge, capacitance, or electric field [20]; at that point, an arbitrary number of spheres can be placed and their radii adjusted to match the desired property of the MSM model to the truth value. Increasing the number of spheres improves the accuracy of the model, but at increased computational cost. Capacitance is a function of the geometry of the object, and is therefore the property used here. Analytical solutions for the capacitance of an object are available for only a select few shape primitives (such as spheres or infinite wires). Therefore, a finite element scheme must be used to find the capacitance of the spacecraft, which can then be used to establish an MSM model that is fast enough for computations.

The MOM is a finite element method that can be used to determine the capacitance of an arbitrary shape. The shape is first discretized into a triangular mesh and the capacitance of each triangular area calculated. Then, the mutual capacitance effects of all other triangular areas in the body on the initial triangle are computed. Repeating this process for each element allows the elastance matrix for the object to be computed [18].

Whereas a significant body of work explores variations of the MSM, including Refs. [18,20, 22,23], this work involved the overall MSM model changing significantly with time, as the two spacecraft approached from tens of meters to tens of centimeters. The MSM formulation is validated for time-varying shapes and structures in [21]. The results of that work mean that the true capacitance of each spacecraft only needs to be computed once, and the MSM model tuned from that truth capacitance is valid across a wide range of conditions.

For the case with two interacting bodies, the elastance matrix $[S]$ can be written in block form as

$$\begin{bmatrix} V_1 \\ V_2 \end{bmatrix} = \begin{bmatrix} S_1 & S_M \\ S_M^T & S_2 \end{bmatrix} \begin{bmatrix} Q_1 \\ Q_2 \end{bmatrix} \tag{10}$$

where the S_M terms refer to the mutual capacitances, the components that vary with the relative positions of the two bodies. Only the mutual capacitances need to be updated at each time step as the spacecraft move relative to each other, and so the MSM sphere radii and the self-capacitance matrices S_1 and S_2 do not need to be recomputed, which saves significant computational effort.

It is again important to note that the structures considered here are assumed to be continuously conducting, as is recommended in design guidelines for mitigating electrostatic charging. However, if the structures were not fully conducting, sections of the spacecraft could develop significantly different potentials, with differential charging resulting in several kilovolt differences across the spacecraft [14].

IV. Charged Proximity Operations Study

All cases here are evaluated with equal potentials on each spacecraft. As both spacecraft are exposed to near-identical environmental conditions (assuming one is not shadowing the other), it is reasonable to assume that each has a similar potential, although there may be differences due to variations in design or material properties. As discussed earlier, the spacecraft are considered to be fully conducting, although this assumption can be reconsidered depending on the specific target vehicle.

The results are organized as follows: first, the electrostatic forces and torques are evaluated for both types of spacecraft as a function of position relative to the target and as a function of potential. As a point of comparison, a basic SRP model considering the spacecraft model facets, but not considering self-shadowing, etc., is used to compare the significance of these perturbations. The impact of electrostatic perturbations in maintaining a static hold relative to a target is then evaluated and fuel consumption compared between an SRP-only case and an SRP and electrostatically perturbed case. The servicer attitude control requirements during these operations are evaluated, and then a full rendezvous scenario with electrostatic perturbations is demonstrated.

A. Electrostatic Force and Torque Magnitudes

As seen in Eq. (9), the electrostatic torque acting on a body is a function of the relative positions of each body, their orientations, the geometry of each body, and the electrostatic potentials. To evaluate the magnitude of electrostatic forces and torques on the target as a function of servicer location, an equidistant shell is developed. Rather than use a spherical shell where each point is an equal distance from the center of mass, each point is distributed such that it is an equal distance from the nearest surface on the target spacecraft, as seen in Fig. 4. The servicer is oriented such that the docking face is oriented toward the target center of mass, enabling comparisons to be drawn between the force and torque on the target at different sample positions. The MSM is used to compute the forces and torques acting on each body. The forces and torques acting on the GOES-R target as a function of servicer azimuth and elevation with a fixed distance from the target are seen in Figs. 5a and 5b.

The maps of torque as a function of azimuth and elevation shown in Figs. 6a and 6b provide some suggestions as to how a trajectory could be designed to minimize the perturbing torque acting on the target.

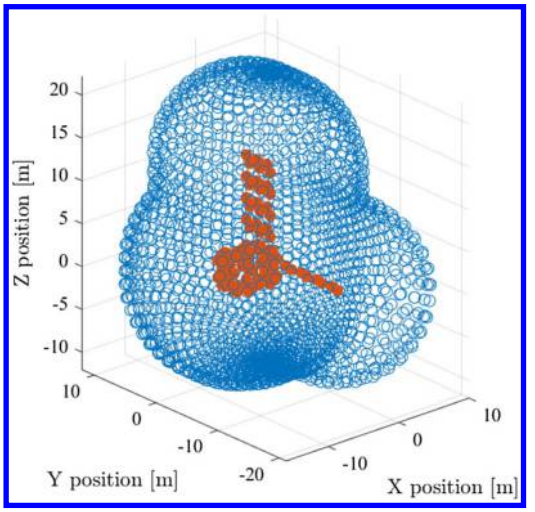

Fig. 4 Sample points of constant distance (10 m) to the spacecraft used to evaluate electrostatic torque on a target as a function of azimuth and elevation.

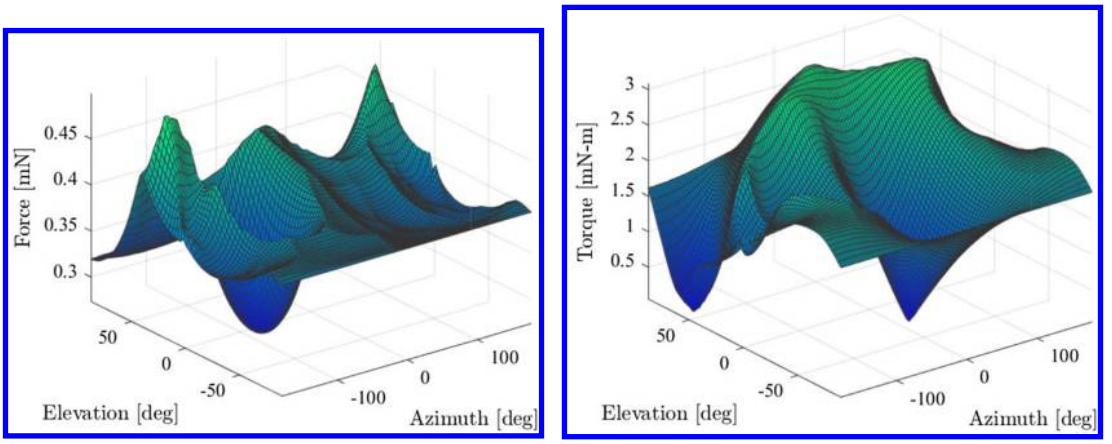

a) Force on GOES-R target for different servicer azimuth and elevations

b) Torque magnitude acting on GOES-R target as a function of servicer position

Fig. 5 Force and torque for different servicer locations, with the servicer at 10 m from the target; all evaluated at 10 kV, with a servicer based on the symmetric two-panel MSM model and a target based on the GOES-R model.

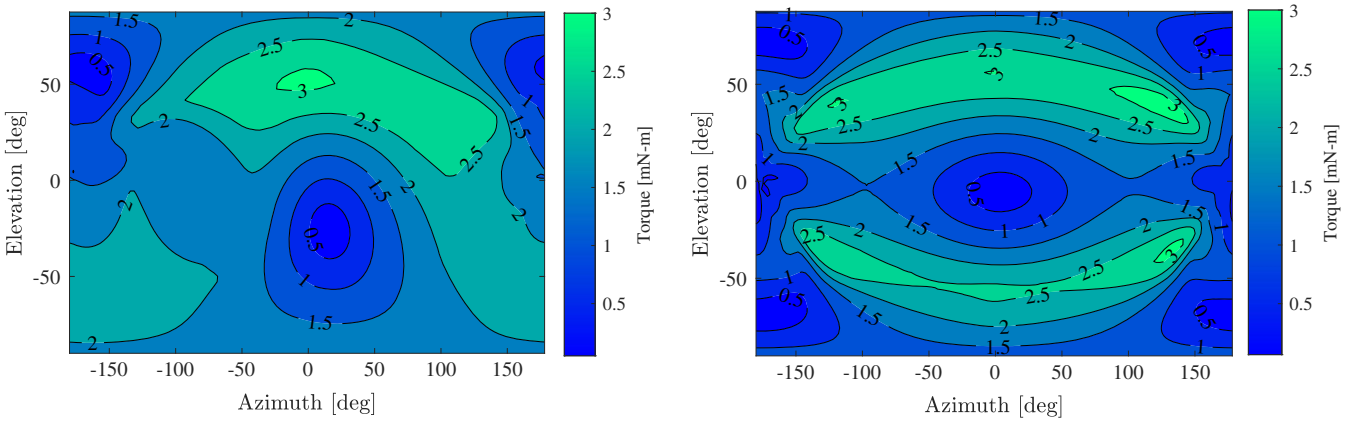

a) Electrostatic torque on GOES-R target

b) Electrostatic torque on two-panel target

Fig. 6 Torque magnitude acting on target as a function of servicer azimuth and elevation, with all positions located 10 m from the target; all points evaluated at 10 kV.

For instance, approach along an azimuth of 15 deg and an elevation of −27 deg decreases the torque imparted to the GOES-R spacecraft by a factor of 20 compared to a straight line approach at 0 deg azimuth and 0 deg elevation. Such an approach may fall within a constraint cone often used during approaches to ensure satisfactory navigation sensor performance and mission safety, and therefore may be acceptable from an operational perspective. Emphasizing the importance of trajectory selection, electrostatic torques can vary by a factor of 50 while maintaining a 25 deg half-angle approach cone constraint for this spacecraft configuration. In most cases of operational constraints imposed on a specific mission, it is possible to develop a feasible trajectory to minimize electrostatic torques.

Minimizing the perturbing torque acting on the target is critical to reducing the acquired rotational rate of the target at grappling, and therefore in reducing control effort required by the servicer and improving safety for the overall mission. In addition to path selection, electrostatic interactions can be minimized by adjusting the attitude of the servicing spacecraft with respect to the target. For the two-panel servicer and GOES-R target scenario, having the spacecraft panels pointing in the same direction results in torques over 30% larger than in a scenario, where the panels are oriented along perpendicular axes. Likewise, altering the orientation of the solar arrays relative to the spacecraft frame will alter the electrostatic torques acting between the spacecraft.

Repeating the equidistant shells procedure for different positional offsets results in Fig. 7, which illustrates the relationship between distance to the target, spacecraft potential, and resultant perturbing torque for both a two-panel and GOES-R target.

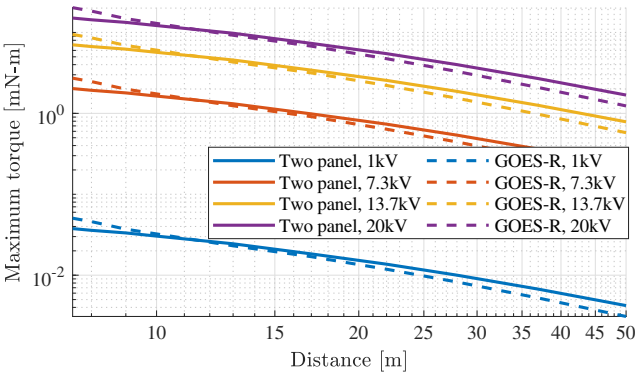

Fig. 7 Maximum electrostatic torque between servicer and target as a function of distance.

B. Comparison to SRP

In high Earth orbits, the dominant perturbation for attitude is typically SRP. As a point of comparison for the significance of the electrostatic forces and torques, a first-order estimate of the SRP-induced torque is investigated. The spacecraft is divided into elements representing each panel in the MOM model in Fig. 3, and a similar procedure is carried out for the two-panel spacecraft model; the front and back of the solar arrays are treated as separate faces to allow different reflection coefficients to be applied to each.

The SRP force per area element is computed as

$$F_i = -P_{\text{SRP}}\left((1-\beta_{s,i})\hat{s} + 2\left(\beta_{s,i}\cos(\theta_i) + \frac{1}{3}\beta_{D,i}\right)\hat{\boldsymbol{n}}_i\right)\cos(\theta_i)A_i \tag{11}$$

where β_s represents the specular reflection coefficient, and β_D is the diffuse reflection coefficient for the given element. The sun-direction unit vector is given by $\hat{\boldsymbol{s}}$, whereas $\hat{\boldsymbol{n}}_i$ is the face normal unit vector; θ_i describes the angle between $\hat{\boldsymbol{s}}$ and $\hat{\boldsymbol{n}}_i$. A_i is the area of the given element.

The specular and diffuse reflection coefficients are taken from Ref. [24], with the spacecraft structure assumed to be covered in multilayer insulation ($\beta_s = 0.29$; $\beta_d = 0.29$), the back of the solar array to be black paint ($\beta_s = 0.015$; $\beta_d = 0.015$), and the front of the solar array to be given by $\beta_s = 0.073$; $\beta_d = 0.007$. Self-shadowing and multiple reflection effects are neglected, and the resultant SRP force and torque are evaluated over a full range of azimuth and elevation angles for the incident sun vector. Torques are computed by treating the SRP force on a given area element as a point force applied to the center of area, with the position vector of the element centroid relative to the center of mass for the spacecraft used to find the resultant torques.

The mean SRP torque on the GOES-R model is found to be about 0.57 mN · m, with a worst-case torque of 1.1 mN · m; the two-panel model had a mean torque of 0.11 mN · m and a worst-case SRP torque of 0.14 mN · m. For the two-panel model, a worst-case torque at 5 m of separation and just 1000 V is sufficient to exceed the maximum SRP torque by a factor of 3; at 10 m, 1900 V results in electrostatic torques exceeding the maximum SRP torque for this body (Fig. 7). Additionally, while SRP forces and torques decrease as the face rotates away from the sun, the electrostatic torques continue to be exerted as long as the servicer is maintaining a relative position, continuing the rotational acceleration of the target. Therefore, the electrostatic perturbations acting on the target are the dominant disturbance at GEO during periods of significant spacecraft charging.

C. Perturbed Station Keeping

To gain further insight into the impact of electrostatic perturbations on proximity operations, a case where the servicer actively maintains a fixed position relative to the target is considered. In this case, the servicer maintains a position 10 m from the target in the Hill-frame $\hat{x}$ direction. Figure 8b shows the trajectory followed by the servicer over this period to maintain a fixed position at 10 m from the target in the target frame. The target is initialized with no rotational motion, but is considered to be inert, and therefore affected by electrostatic perturbations. Each hold is evaluated over an arbitrary 5 h period.

1. Controller Description

A Lyapunov-derived reference tracking controller is implemented to follow a desired trajectory, such as a position fixed in the target body frame $\mathcal{T}$, computing the required control authority as [19]

$$u = -\left(f(r_d) - f(r_{d_d})\right) - [K_1]\Delta r - [K_2]\Delta\dot{r} \tag{12}$$

where Δr represents the difference between the spacecraft actual position and the desired position in the reference frame of the target, and $\Delta\dot{r}$ represents the velocity difference in the same frame. The term $(f(r_d) - f(r_{d_d}))$ represents the relative inertial acceleration between the vehicle and the target orbit, evaluated numerically at each time step. To mimic a servicer case, where the spacecraft potentials are unknown, this relative acceleration term includes only relative accelerations due to gravity, not the electrostatic perturbations. The gain matrices $[K_1]$ and $[K_2]$ are set to achieve desired performance, with $[K_1] = 0.03 \cdot [I_{3\times3}]$ and $[K_2] = 3 \cdot [I_{3\times3}]$ to achieve a closed-loop response time on the order of minutes while avoiding thruster saturation, representative of such a rendezvous scenario.

The goal of this work was to evaluate the contribution of specifically electrostatic perturbations, and so navigational or controller noise is not included in simulations and perfect knowledge of relative states assumed. However, the control authority is limited to account for thruster saturation effects. For the MEV-1 mission, final approach and rendezvous control was provided by a mix of 1 and 22 N hydrazine thrusters developed by Aerojet Rocketdyne; given a spacecraft mass of approximately 2300 kg, the 22 N thrusters set an upper acceleration limit of ~0.01 m/s^2, which is used here [25]. The attitude of the servicer is prescribed to match the attitude of the target, ensuring docking faces remained aligned.

2. Station Keeping Results

Although it is expected that the case of an asymmetrical target like the GOES-R spacecraft would experience significant electrostatic torques, it is possible for symmetric targets to experience these perturbations as well. More generally, any case where the electrostatic force vector is not colinear with the vector from the servicer COC to the target center of mass will result in a net torque on the

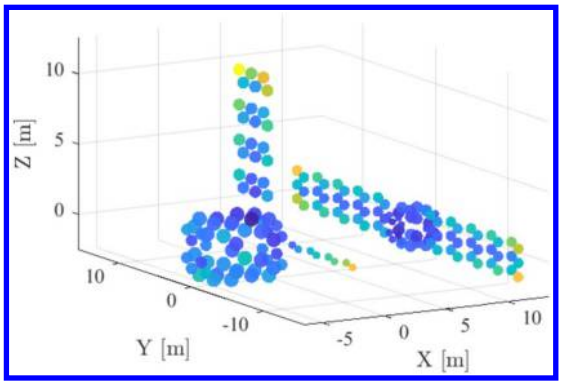

a) Servicer (right) at a 10 meter hold point relative to the target (left), both craft at 0 kV

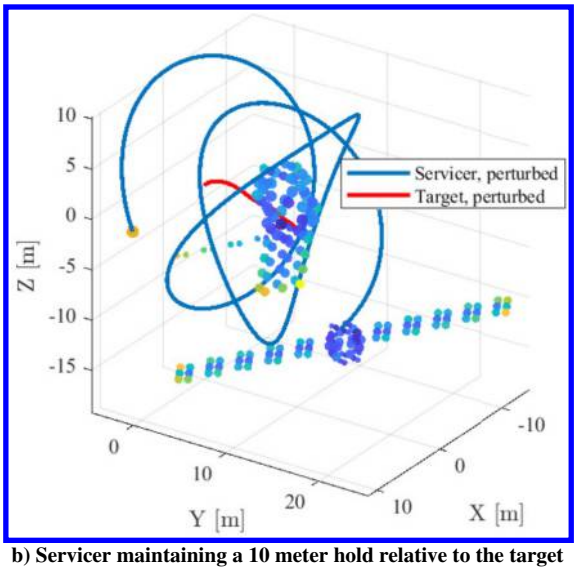

b) Servicer maintaining a 10 meter hold relative to the target for 5 hours, both craft at 10 kV; Only electrostatic perturbations acted on the target

Fig. 8 Results of servicer holding a fixed position relative to a target for a 5 h hold, shown in the Hill frame; electrostatic torques result in a significant tumble being imparted to the target, despite it having no initial rotation.

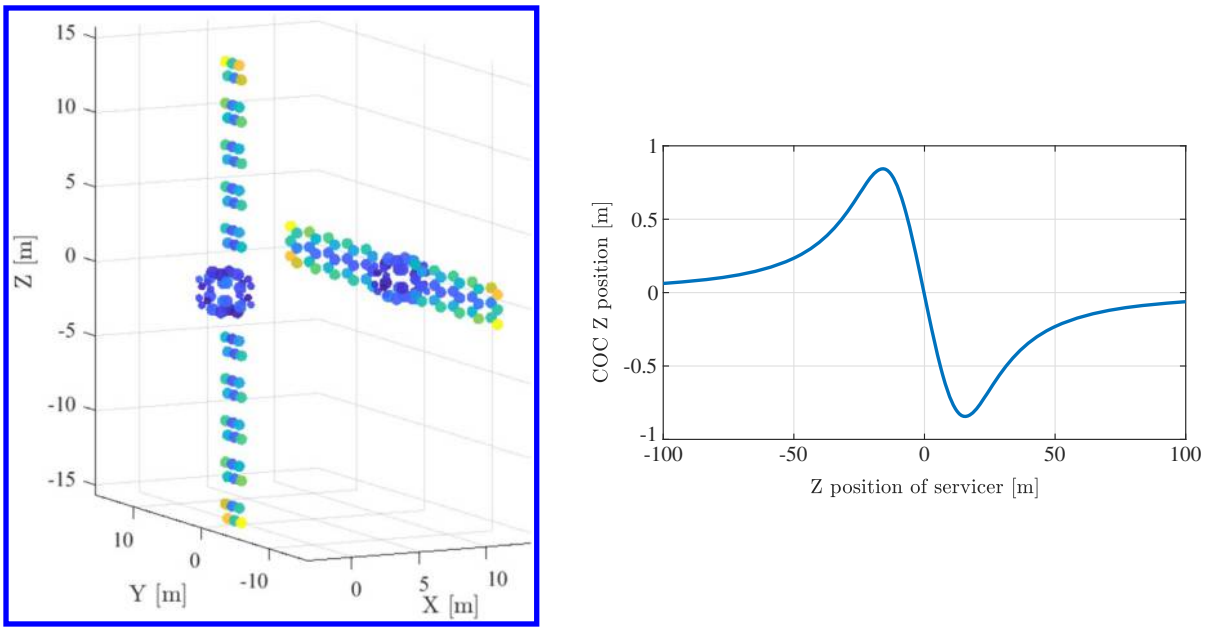

a) Initial position of servicer (right) and two-panel target (left); Target is centered at the origin, servicer is offset by 10 m in the X direction

b) Change in center of charge (CoC) position of the target as a function of servicer location

Fig. 9 Variation in target parameters with changing servicer position.

target. Because of mutual elastance effects, as one charged body approaches another, the COC location of each body will change. Figure 9b shows how the Z position of the COC of a symmetrical spacecraft is impacted by the relative position of a nearby object. For this case, where both craft were held at 10 kV potentials, the COC position is shifted by up to ± 85 cm by induced capacitance effects of the nearby servicer.

A sweep of parameters is run to quantify the increase in control effort caused by the electrostatic perturbations for the hold case with an asymmetric GOES-R target. The target spacecraft was assumed to be inert and the servicer required to maintain a fixed position relative to the target. The ΔV required to hold a fixed position relative to the target when perturbed by only SRP is compared to the ΔV requirement when both SRP and electrostatic perturbations are present. These simulations use the same x offset for the hold point in the target frame (10 m), but varied the $\hat{z}$ position, from the target spacecraft docking location up to the top of the solar array of the target. This allows the impact of relative position on control effort to be evaluated, as moving the servicer COC further from the center of mass of the target will result in larger effective torques. This trend can be seen in the resulting control effort increase with increasing $\hat{z}$ position seen in Fig. 10.

Even when the servicer is aligned with the docking port of the two-panel target at $z = 0$ m, the torques generated by -10 kV potentials result in a control effort increase of over three times the SRP-only perturbed case at 10 m separation, whereas a hold level with the top of the solar array yields an increase of over 10 times the unperturbed case. Additionally, the acceleration required by the servicer to maintain a position 10 m away from the target at 10 kV reached approximately 1 mm/s^2, which could saturate the 1 N thrusters used as part of the fine maneuvering system on MEV-1 or a future servicing mission [25]. These numbers demonstrate that proximity operations can be significantly perturbed by electrostatic interactions.

Interestingly, there are combinations of potential and position, which decrease the fuel consumption relative to the SRP-only perturbation case. This is a result of the electrostatic torques countering the SRP-induced torques, yielding reductions in final rotational rate of over 50% compared to the SRP-only case, and corresponding fuel savings of over 30% (Fig. 10a).

D. Servicer Attitude Control Requirements

As the target tumbles, the servicer must both translate and rotate to maintain a fixed relative orientation. The attitude of the servicer is prescribed to match that of the target in this scenario, but the torque required to achieve this rotation can be computed at each time step by rearranging Eq. (2).

The inertia matrix is taken to be the same as the one estimated for the GOES-R spacecraft, as an estimate for a generic large GEO spacecraft. Figure 11 shows the torque required for the servicer to maintain its orientation relative to the target during the hold at different Z positions and potentials. Increasing the Z offset away from the

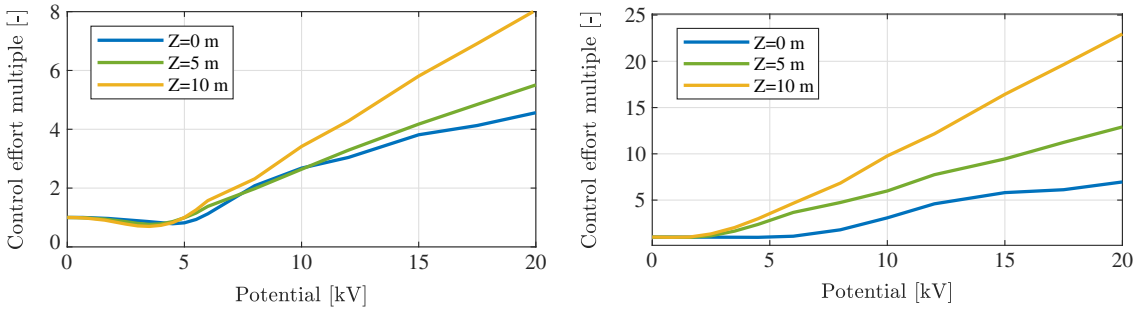

a) Control effort multiple with asymmetric GOES-R target

b) Control effort multiple with symmetric two-panel target

Fig. 10 Increase in control effort (as a multiple of the ΔV for the 0 V SRP-only case) required to hold a fixed 10 m offset from the target for different servicer $\hat{z}$ positions.

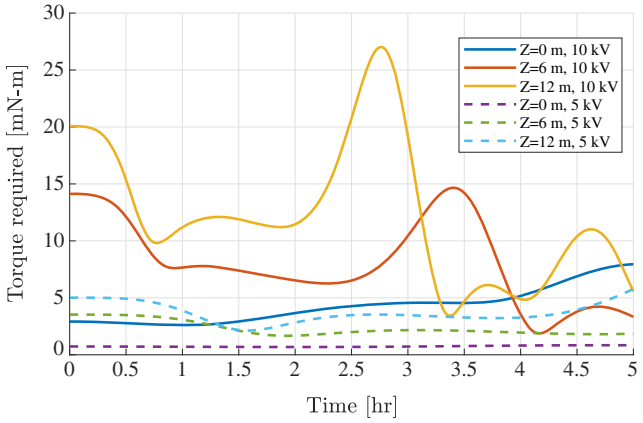

Fig. 11 Torque required by servicer to maintain a relative orientation to the GOES-R target while holding a 10 m offset position and 10 kV on each spacecraft.

target spacecraft centerline results in higher torque requirements for the servicer, as does increasing the potential of the spacecraft from 5 to 10 kV. In both cases, these changes increase the torque acting on the target, and so it is logical for the servicer to then require higher torque levels to maintain relative attitude. The highest required torque, for the $Z = 12$ m and 10 kV potential case, is over 27 mN · m. Large reaction wheels, such as the Honeywell HR12, are capable of generating torques of 100–200 mN · m, suggesting that these torques are significant but achievable [26]. The accumulated momentum in the reaction wheels as a result of these attitude maneuvers could present another limiting factor in control during charged proximity operations.

V. Rendezvous Example

Although it is clear that there can be force and torque perturbations as a result of electrostatic interactions, it is less clear how much they might realistically matter in a rendezvous scenario, where a relatively limited time is spent in close proximity to the target. To simulate this scenario, a nominal rendezvous trajectory is developed based on public videos of the MEV-1 final trajectory. The servicer begins 80 m from the target and follows a straight trajectory to the interface point. Several holds are built in along the way, with 10 min each at 20, 10, and 3 m from the target. The terminal point is 1 m from the docking location, at which point physical grasping mechanisms take over during a final 30 min hold.

A precomputed reference trajectory (shown in Fig. 12) is used here, and the controller tracks the reference as it evolves with time. The inherently coupled dynamics of the two spacecraft can increase the risk of collision, as induced torques on the target spacecraft can result in collisions between antennas or arrays on the target and the servicer. In these cases, it may only take a few degrees of target rotation to cause contact with the servicer.

The controller gains prioritize tracking accuracy as might be expected for the terminal rendezvous phase in an operational mission, where positioning may be valued above fuel consumption concerns. These gains ($[K_1] = 0.03 \cdot [I_{3\times3}]$ and $[K_2] = 3 \cdot [I_{3\times3}]$) are selected to avoid saturating the controllers, but still enabling high-precision rendezvous with a nominal fuel cost of 0.11 m/s when only gravitationally induced relative motion perturbs the relative trajectory.

Because the controller is forced to track a reference position that is accelerating in an inertial frame when the target begins to rotate, a steady-state equilibrium is not possible, and therefore, performance with respect to steady-state errors cannot be evaluated. However, for this rendezvous scenario, adding a −1 kV potential to each spacecraft results in an 80-fold increase in fuel consumption (compared to a case with only gravitational accelerations), comparable to a worst-case SRP addition. The addition of −1 kV potentials to a case already perturbed by SRP can, as observed with the static hold cases, either increase or decrease control effort required for rendezvous by up to 10%.

Increasing the potential to just −5 kV results in over 30% increase in fuel consumption to maintain millimeter-level errors in final position (relative to a worst-case SRP perturbation), and the target acquires rotational rates of 0.03 deg/s prior to rendezvous. Spacecraft potentials of −10 kV, seen in Fig. 13, are still within the capability of the control system to maintain accurate positioning, with a worst-case error of just over 3 cm, but at considerable fuel cost: over 9 m/s or 125% increase over the maximum-SRP reference case (and over 90 times more than an unperturbed case). The target experiences more than a complete tumble during this rendezvous and final rotational rates of 0.05 deg/s. Finally, a near-record electrostatic charging level of −20 kV on each spacecraft results in a nearly 300-fold increase in control effort, worst-case positioning errors of 20 cm, and final target rotational rates of 0.2 deg/s.

VI. Conclusions

Ultimately, these results demonstrate that charging conditions that have been observed at GEO present significant perturbations to proximity operations and should be modeled in rendezvous and proximity operations development. Perturbing torques between modeled spacecraft at 10 kV are shown to be an order of magnitude larger

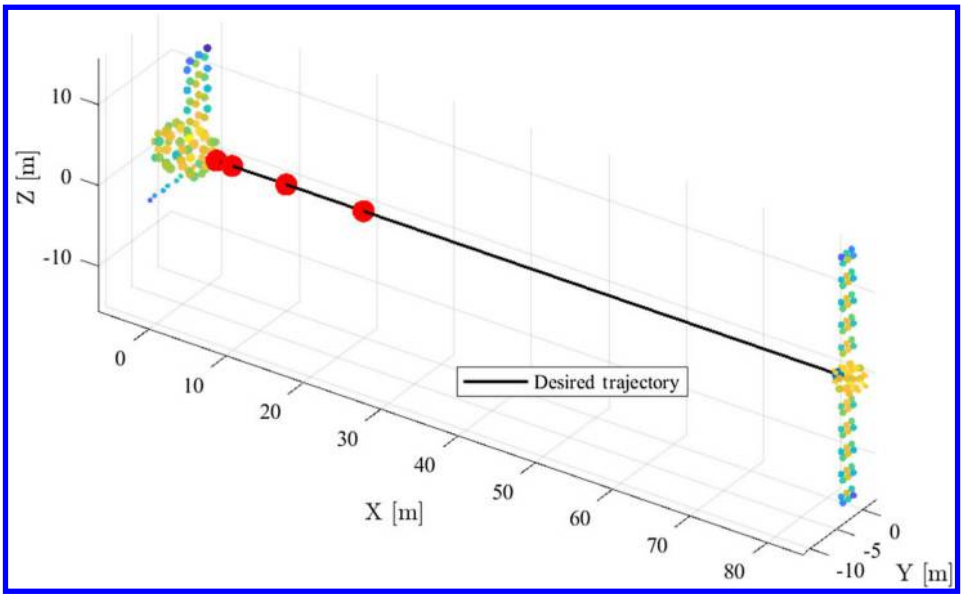

Fig. 12 Reference trajectory from the servicer (right) to the disabled target (left); the hold points are shown as red dots.

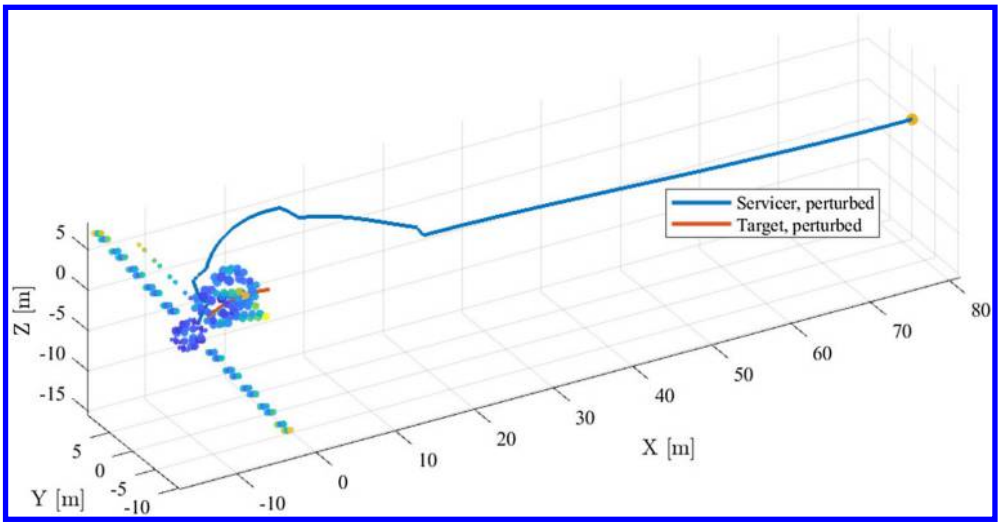

Fig. 13 Perturbed rendezvous trajectory with −10 kV potential on each spacecraft.

than SRP and can dramatically increase the control effort required to perform proximity operations. These perturbing effects exist even when the potential between the spacecraft has been equalized, such as through the use of a plasma contactor (although the injection of plasma may introduce additional shielding effects between the spacecraft, and should be further considered).

For some cases, such as a servicer that must inspect or repair a solar array, or a significantly asymmetric target object, it will be impossible to avoid imparting disturbing torques to the target. However, changing the attitude of the servicer on approach, or altering solar array orientations, may help in minimizing these torques. Developing control and guidance strategies to feedforward on estimates of electrostatic potentials on each spacecraft to improve proximity operations perturbed by charging will be a goal of future work.

The examples presented here are not bounding cases, but instead serve to illustrate a possible scenario during a rendezvous that is not designed to account for electrostatic interactions. Worst-case scenarios depend on the specific spacecraft geometries, approach trajectory, and electrostatic potentials on each spacecraft. Although electrostatic torques tend to increase fuel consumption and complicate rendezvous, in some cases the electrostatic torques can be helpful by balancing SRP torques, reducing overall fuel consumption and terminal rotational rate. This suggests appropriate selection of a rendezvous or proximity operation trajectory, and accurate knowledge of the potentials on both spacecraft is crucial to mitigating the impact of these perturbations, or could even use these perturbations to impart desired torques on the target.

Acknowledgment

This work was supported through the U.S. Air Force Office of Scientific Research grant #FA9550-20-1-0025.

References

[1] Clark, S., "Two Commercial Satellites Link Up in Space for First Time," Spaceflight Now, 2020, https://spaceflightnow.com/2020/02/26/two-commercial-satellites-link-up-in-space-for-first-time/.

[2] Reed, B. B., Smith, R. C., Naasz, B. J., Pellegrino, J. F., and Bacon, C. E., "The Restore-L Servicing Mission," *AIAA SPACE Forum 2016*, AIAA Paper 2016-5478, Sept. 2016. https://doi.org/10.2514/6.2016-5478

[3] Karavaev, Y. S., Kopyatkevich, R. M., Mishina, M. N., Mishin, G. S., Papushev, P. G., and Shaburov, P. N., "The Dynamic Properties of Rotation and Optical Characteristics of Space Debris at Geostationary Orbit," *Advances in the Astronautical Sciences*, Vol. 119, Jan. 2004.

[4] Lai, S. T., *Fundamentals of Spacecraft Charging: Spacecraft Interactions with Space Plasmas*, Princeton Univ. Press, Princeton, NJ, 2011, Chaps. 2, 3, 5.

[5] Anderson, P. C., "Characteristics of Spacecraft Charging in Low Earth Orbit," *Journal of Geophysical Research*, Vol. 117, No. A7, 2012, Paper A07308. https://doi.org/10.1029/2011 JA016875

[6] Olsen, R., "The Record Charging Events of ATS-6," *Journal of Spacecraft and Rockets*, Vol. 24, No. 4, 1987, pp. 362–366. https://doi.org/10.2514/3.25925

[7] Seubert, C. R., Stiles, L. A., and Schaub, H., "Effective Coulomb Force Modeling for Spacecraft in Earth Orbit Plasmas," *Advances in Space Research*, Vol. 54, No. 2, 2014, pp. 209–220. https://doi.org/10.1016/j.asr.2014.04.005

[8] King, L. B., Parker, G. G., Deshmukh, S., and Chong, J.-H., "Spacecraft Formation-Flying Using Inter-Vehicle Coulomb Forces," NASA/NIAC, Jan. 2002, http://www.niac.usra.edu/files/studies/final_report/601King.pdf.

[9] King, L. B., Parker, G. G., Deshmukh, S., and Chong, J.-H., "Study of Interspacecraft Coulomb Forces and Implications for Formation Flying," *Journal of Propulsion and Power*, Vol. 19, No. 3, 2003, pp. 497–505. https://doi.org/10.2514/2.6133

[10] Schaub, H., and Moorer, D. F., "Geosynchronous Large Debris Reorbiter: Challenges and Prospects," *Journal of the Astronautical Sciences*, Vol. 59, Nos. 1–2, 2014, pp. 161–176.

[11] Bengtson, M., Wilson, K., Hughes, J., and Schaub, H., "Survey of the Electrostatic Tractor Research for Reorbiting Passive GEO Space Objects," *Astrodynamics*, Vol. 2, No. 4, 2018, pp. 291–305. https://doi.org/10.1007/s42064-018-0030-0

[12] Ozkul, A., Lopatin, A., and Shipp, A., "Initial Correlation Results of Charge Sensor Data from Six Intelsat VIII-Class Satellites with Other Space and Ground Based Measurements," *Proceedings of the Seventh International Conference*, European Space Agency, ESA SP-476, R. A. Harris, Nov. 2001, p. 293.

[13] Nose, M., Iyemori, T., Sugiura, M., and Kamei, T., "Kp Index," World Data Center for Geomagnetism, Kyoto, 2020, http://wdc.kugi.kyoto-u.ac.jp/kp/index.html#LIST [retrieved 10 Oct. 2020].

[14] Olsen, R. C., McIlwain, C. E., and Whipple, E. C., Jr., "Observations of Differential Charging Effects on ATS 6," *Journal of Geophysical Research: Space Physics*, Vol. 86, No. A8, 1981, pp. 6809–6819. https://doi.org/10.1029/JA086iA08p06809

[15] Purvis, C. K., Garrett, H. B., Whittlesey, A. C., and Stevens, N. J., "Design Guidelines for Assessing and Controlling Spacecraft Charging Effects," NASA TR 2361, 1984.

[16] Ferguson, D. C., and Hillard, G. B., "New NASA SEE LEO Spacecraft Charging Design Guidelines—How to Survive in LEO Rather Than GEO," NASA TM—2003-212737, Dec. 2003.

[17] Anon., "GOES-R Series Data Book," NASA GOES-R Series Program Office TR, 2019, https://www.goes-r.gov/downloads/resources/documents/GOES-RSeriesDataBook.pdf.

[18] Hughes, J. A., and Schaub, H., "Heterogeneous Surface Multisphere Models Using Method of Moments Foundations," *Journal of Spacecraft and Rockets*, Vol. 56, No. 4, 2019, pp. 1259–1266. https://doi.org/10.2514/1.A34434

[19] Schaub, H., and Junkins, J. L., *Analytical Mechanics of Space Systems*, 4th ed., AIAA Education Series, AIAA, Reston, VA, 2019, Chaps. 3, 4, 8.

[20] Stevenson, D., and Schaub, H., "Multi-Sphere Method for Modeling Electrostatic Forces and Torques," *Advances in Space Research*, Vol. 51, No. 1, 2013, pp. 10–20.
https://doi.org/10.1016/j.asr.2012.08.014

[21] Maxwell, J., Wilson, K., Hughes, J., and Schaub, H., "Multisphere Method for Flexible Conducting Space Objects: Modeling and Experiments," *Journal of Spacecraft and Rockets*, Vol. 57, No. 2, 2020, pp. 225–234.
https://doi.org/10.2514/1.A34560

[22] Engwerda, H., "Remote Sensing for Spatial Electrostatic Characterization Using the Multi-Sphere Method," Master's Thesis, Delft Univ. of Technology, Delft, The Netherlands, March 2017.

[23] Chow, P., Hughes, J., Bennett, T., and Schaub, H., "Automated Sphere Geometry Optimization for the Volume Multi-Sphere Method," *AAS/AIAA Spaceflight Mechanics Meeting*, AAS Paper 17-451, San Antonio, TX, Feb. 2017.

[24] List, M., Bremer, S., Rievers, B., and Selig, H., "Modelling of Solar Radiation Pressure Effects: Parameter Analysis for the MICROSCOPE Mission," *International Journal of Aerospace Engineering*, Vol. 2015, Jan. 2016, Paper 928206.
https://doi.org/10.1155/2015/928206

[25] Anon., "Aerojet Rocketdyne Propulsion Helps Enable New Satellite Servicing Market," Aerojet Rocketdyne TR, 2020, https://www.rocket.com/media/news-features/ar-propulsion-helps-enable-new-satellite-servicing-market.

[26] Marshall, T., and Fletcher, M., "Meeting High-Quality RWA Commercial Demand Through Innovative Design," *Proceedings of the 8th European Symposium*, Vol. 438, Space Mechanisms and Tribology, European Space Agency, ESA-SP, 1999, p. 253.

D. P. Thunnissen
Associate Editor